

# Isospin Transport at Fermi Energies

V.Baran<sup>1,2</sup>, M.Colonna<sup>1</sup>, M.Di Toro<sup>1</sup>, M.Zielinska-Pfabé<sup>3</sup> and H.H.Wolter<sup>4</sup>

<sup>1</sup> *Laboratori Nazionali del Sud, Via S. Sofia 44, I-95123 Catania, Italy*

*and Physics-Astronomy Dept., University of Catania*

<sup>2</sup> *NIPNE-HH, Bucharest and Bucharest University, Romania*

<sup>3</sup> *Smith College, Northampton, MA 01063, USA and*

<sup>4</sup> *Dept. Physik, University of Munich, 85748 Garching, Germany*

(Dated: August 16, 2018)

In this paper we investigate isospin transport mechanisms in semi-peripheral collisions at Fermi energies. The effects of the formation of a low density region (neck) between the two reaction partners and of pre-equilibrium emission on the dynamics of isospin equilibration are carefully analyzed. We clearly identify two main contributions to the isospin transport: isospin diffusion due to the  $N/Z$  ratio and isospin drift due to the density gradients. Both effects are sensitive to the symmetry part of the nuclear Equation of State (EOS), in particular to the value and slope around saturation density.

keywords: Isospin transport; Binary collisions; Neck Dynamics; Symmetry energy.

PACS numbers: 21.30.Fe, 25.70.-z, 25.70.Lm, 25.70.Pq.

## I. INTRODUCTION

In the last few years the increased accuracy of the experimental techniques has renewed interest in nuclear reactions at Fermi energies. Exclusive measurements, event-by-event analysis, and a  $4\pi$  coverage allow a deeper investigation of the evolution of the reaction mechanisms with beam energy and centrality. New insights into the understanding of the nuclear matter equation-of-state (*EOS*) were gained [1]. In particular, recent experimental and theoretical analyses were devoted to the study of the properties and effects of the symmetry term of the *EOS* (asy-*EOS*) away from saturation conditions [2, 3].

Indeed, the two-component character of nuclear matter adds some special interest to the dynamics of heavy ion collisions at intermediate energies, between 20 and 100 AMeV. In *central* collisions isospin distillation is an important effect in multifragmentation of charge asymmetric systems. Here phase separation is driven by isoscalar-like unstable fluctuations, i.e. local in phase variations of proton and neutron densities [4, 5, 6, 7]. This leads to a more symmetric “liquid” phase of fragments surrounded by a more neutron rich “gas” relative to the original asymmetry of the system. Isoscaling phenomena, observed experimentally, provide indications for such a scenario [8, 9].

In *semi-peripheral* collisions between nuclei with different  $N/Z$  ratio, isospin dynamics will drive the system toward a uniform asymmetry distribution. The degree of equilibration, correlated to the interaction time, should provide some insights into transport properties of fermionic systems [10, 11], in particular give information on transport coefficients of asymmetric nuclear matter [12, 13].

The aim of this work is to investigate the isospin transfer through the neck region in semi-peripheral collisions

of asymmetric nuclei at Fermi energies. Of particular interest is the role of the density dependence of the symmetry energy in this process. The isospin transfer was measured for collisions of different *Sn* isotopes at MSU [14, 15, 16] and interpreted theoretically with the result that the asy-*EOS* should be rather stiff. In these works the effect of pre-equilibrium emission, which changes the isospin content of the interacting system, was not analyzed explicitly. Here we will discuss this questions in detail, as well as the different transport processes affecting the final isospin content. Quantitatively, dynamical isospin effects can be properly understood only from microscopic calculations based on transport models. We will base our study on a stochastic BNV transport model (see refs. [17, 18] for more details on the main ingredients of this approach).

## II. ISOSPIN EQUILIBRATION PROCESS

We are focusing on the charge asymmetric collision  $^{124}Sn + ^{112}Sn$ , at 50 AMeV bombarding energy, to which we refer as the mixed system, (*M*). To investigate the density ( $\rho$ ) dependence we consider here two representative parameterizations of the symmetry energy,  $E_{sym}(\rho, I)/A = C_{sym}(\rho)I^2, I = (N - Z)/A$ : one showing a rapidly increasing behaviour with density, roughly proportional to  $\rho^2$  (asyssuperstiff) and one where a kind of saturation is observed above normal density (soft, *SKM\**) (see Ref.[3, 6] for more detail).

The BNV simulations have been performed for semi-peripheral collisions at impact parameters  $b = 6, 8, 9, 10 fm$ . In the last two cases the reaction has dominantly a binary character and the charge asymmetry of primary projectile (target)- like fragments, *PLF* (*TLF*), should provide the essential information about the isospin equilibration rate. At  $b = 8 fm$  already about 25% of the events are ternary. An IMF can be formed in the mid-velocity region by neck fragmentation [19]. For more central events this mechanism becomes dominant: at  $b = 6 fm$ , one or two IMF's are found in

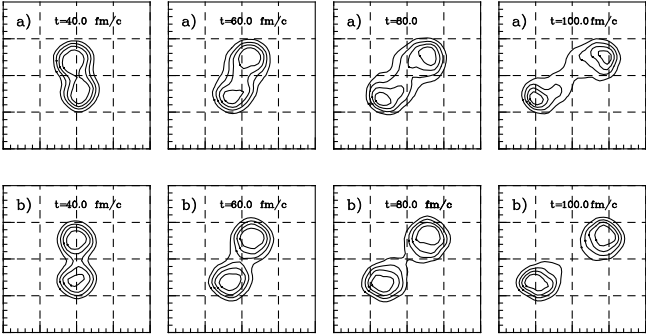


FIG. 1:  $^{124}\text{Sn} + ^{112}\text{Sn}$   $b = 8\text{fm}$  (upper row) and  $b = 10\text{fm}$  (lower row) collision: density contour plots. The side of each box is 40 fm.

more than 70% of events [6]. The fragment formation in the neck region will influence the final isospin distribution of the PLF/TLF, and will render considerably more difficult the interpretation of the results. Thus in the following we select only binary events in our analysis. We define the average interaction time,  $t_c$ , as the time elapsed between the initial touching and the moment when *PLF* and *TLF* reseparate. From our simulations we obtain  $t_c \approx 140, 120, 100, 80\text{fm}/c$  for the impact parameters  $b = 6, 8, 9, 10\text{fm}$ , respectively. Four hundred events were calculated for each initial condition and for each asy-*EOS*.

Typical density contour plots, at  $b = 8\text{fm}$  and  $b = 10\text{fm}$ , are shown in Figure 1. We note the dynamical evolution of the overlap region: driven by the fast leading motion of *PL*- and *TL*- prefragments, the formation of a lower density interface can be clearly observed after around  $40\text{fm}/c$ . An isospin migration, or transport, takes place during this transient configuration of two residues with densities close to the normal one, separated by a dilute neck region. In contrast, in deep-inelastic collisions at lower energies the isospin equilibration is driven by the N/Z difference between the interacting nuclei having a quite uniform density profile without a low density interface until separation [20].

We quantify the degree of equilibration by the isospin transport (imbalance) ratio [21], defined as:

$$R_i = \frac{2I_i^M - I_i^H - I_i^L}{I_i^H - I_i^L} \quad (1)$$

Here  $i = P, T$  stands for the projectile-like (target-like) fragment. The quantities  $I_i$  refer to the isospin,  $I = (N - Z)/A$ , or in general to any isospin dependent quantity, characterizing the fragments at separation time, for the mixed reaction ( $M, 124 + 112$ ), the reactions between neutron rich ( $H, 124 + 124$ ), and between neutron poor nuclei ( $L, 112 + 112$ ), respectively. A value of  $R_i$  approaching zero is an indication of a larger degree of equilibration. The extreme cases  $R_T = -1$  and  $R_P = 1$  correspond to the absence of any isospin transfer.

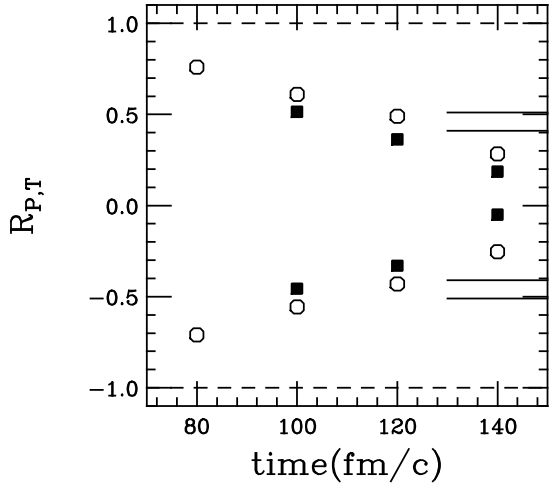


FIG. 2: The isospin transport ratio  $R_{P,T}$ , eq. (1), for the asysoft (full squares) and asysuperstiff (circles) *EOS*'s as a function of the interaction time  $t_c$ , corresponding to different impact parameter  $b$ . The band between the two solid lines corresponds to the experimental data of [15, 16].

The results of the calculations are shown in Figure 2 for the dependence of  $R_{P/T}$  on the interaction time  $t_c$  for the asysoft (squares) and asysuperstiff (circles) *EOS*'s. The figure also shows the experimental values extracted in ref. [15, 16] at semi-peripheral collisions at about  $b = 8\text{fm}$ . We conclude, as in ref. [15], that an asystiff-like *EOS* provides a better agreement with the experimental observations.

A significant difference between the two equations of state is evident for larger interaction times, i.e. smaller values of the impact parameter,  $b = 6, 8\text{fm}$ . The smaller values of isospin transport ratios for the asysoft *EOS* point toward a faster equilibration rate. In refs. [15, 22] an explanation was based on the observation that below normal density the asysoft *EOS* has a larger value of the symmetry energy. Therefore an enhanced isospin equilibration will occur if the diffusion takes place at uniform lower density. We intend to show, that in fact the mechanism of charge equilibration is more complicated due to dynamical evolution of the reaction at these energies. Fast particle emission and density gradients will also play a role. In the next section we investigate more in detail the various influences on the isospin transfer process.

### III. ISOSPIN SHARING AT FERMI ENERGIES

The isospin content of the two residues in a mixed collision system at separation time is determined by the interplay between the particle emission to the gas from each nucleus during the overlap and the transfer of nucleons through the neck. We thus write simple balance equations:

$$I_P = \frac{A_P^0}{A_P} (I_P^0 - \frac{A_{gP}}{A_P^0} I_{gP} - \frac{A_{PT}}{A_P^0} I_{PT} + \frac{A_{TP}}{A_P^0} I_{TP}) \quad (2)$$

$$I_T = \frac{A_T^0}{A_T} (I_T^0 - \frac{A_{gT}}{A_T^0} I_{gT} + \frac{A_{PT}}{A_T^0} I_{PT} - \frac{A_{TP}}{A_T^0} I_{TP}) \quad (3)$$

Here  $I_P$  ( $I_T$ ) and  $A_P$  ( $A_T$ ) are the *PLF* (*TLF*) asymmetry and mass at separation,  $I_P^0$  ( $I_T^0$ ) and  $A_P^0$  ( $A_T^0$ ) the initial projectile (target) asymmetry and mass. Then  $I_{gP}$  ( $I_{gT}$ ),  $A_{gP}$  ( $A_{gT}$ ) are the asymmetries and masses of the projectile/target “gas”, i.e. of the pre-equilibrium particles emitted by the projectile (target) during the interaction time. Finally  $I_{PT}$  ( $I_{TP}$ ), and  $A_{PT}$  ( $A_{TP}$ ) are the asymmetry and mass of all nucleons transferred from projectile (target) to target (projectile).

In Figure 3 we plot the time evolution of the quantities  $I_{gP}$ ,  $I_{gT}$  and  $A_{gP}$ ,  $A_{gT}$ , as well as the values of  $I_{PT}$  and  $I_{TP}$  for the asysoft and the asysuperstiff *EOS* for two impact parameters. We note that  $I_{gP}$  is much larger than  $I_P^0$ . The same is true for the target but the difference is smaller. Thus the pre-equilibrium emission reduces the  $N/Z$  difference between the two nuclei, competing with the transfer process. This is also clearly seen in Figure 4 where the time evolution of the projectile, target, and composite system apparent asymmetry,  $I_P^{app}$ ,  $I_T^{app}$  and  $I_C^{app}$  is shown. The apparent asymmetry is calculated taking into account only the preequilibrium emission but not the isospin transfer inside the matter. A stronger variation is observed for the neutron rich projectile. The composite system asymmetry,  $I_C^{app}$ , is the limiting value toward which the two participants would evolve in complete isospin equilibrium. In contrast, we show in the figure the final asymmetries  $I_P$  and  $I_T$  including the transfer processes.

Comparing the results for the two *EOS*’s in Figs. 3 and 4 we see that a more neutron rich composition of pre-equilibrium emission is generated in the asysoft case because below normal density, from where most of the emitted nucleons originate, the neutrons (protons) are less (more) bound than for the asysuperstiff *EOS*. The differences between the two asy-*EOS*’s are strongly reduced at larger impact parameters, as seen in the results for  $b = 10\text{ fm}$  in Figures 3 and 4, since the interaction times are much shorter.

We next show in Figure 5 the dependence of the quantities introduced above on interaction time, i.e. impact parameter. Here the projectile (target) and gas final asymmetries  $I_P$ ,  $I_{gP}$  ( $I_T$ ,  $I_{gT}$ ) are confronted with the transferred asymmetries  $I_{PT}$  and  $I_{TP}$ . For the projectile, that is neutron rich, both pre-equilibrium emission and nucleon transfer drive the system toward a more symmetric configuration (left). The two processes have opposite effects and thus tend to compensate for the target (right). Therefore the projectile asymmetry has a more pronounced deviation from the corresponding initial value in comparison to the target.

We find a clear dependence on the asy-*EOS* of the isospin transferred between the two nuclei. In particular,

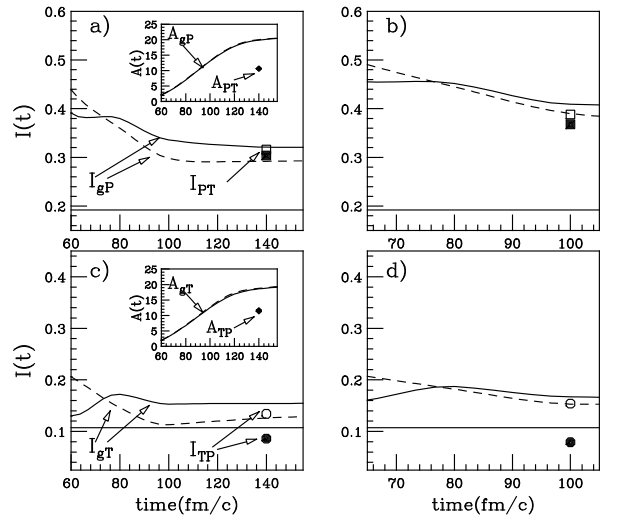


FIG. 3:  $^{124}\text{Sn} + ^{112}\text{Sn}$  collision at  $b = 8\text{ fm}$  (left) and  $b = 10\text{ fm}$  (right): Time evolution of isospin content and mass of preequilibrium particles  $I_{gP}$ ,  $A_{gP}$  ( $I_{gT}$ ,  $A_{gT}$ ) emitted from the projectile (top panels) (resp. target, lower panels) for asysoft (solid lines) and asysuperstiff (dashed lines) *EOS*. The squares (circles) indicate the mass and isospin of the nucleons that have migrated from projectile to target  $I_{PT}$  (and vice versa,  $I_{TP}$ ) for asysoft (full symbols) and asysuperstiff (empty symbols) at separation time. The horizontal lines in the left panels give the initial isospin of the projectile,  $I_P^0$ , and target,  $I_T^0$ , respectively.

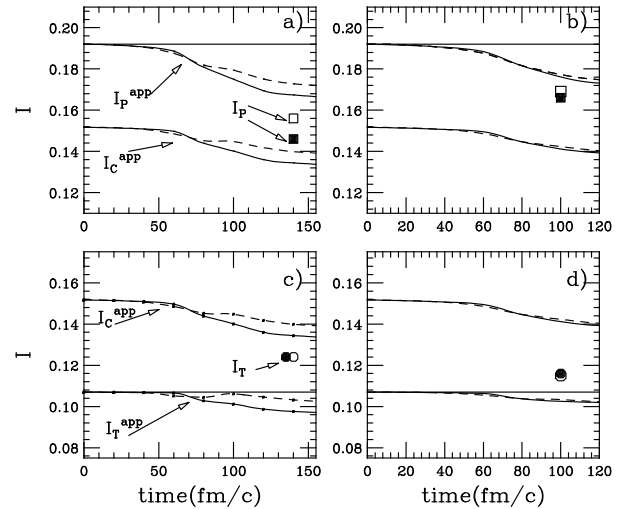


FIG. 4:  $^{124}\text{Sn} + ^{112}\text{Sn}$  at  $b = 8\text{ fm}$  (left windows) and  $b = 10\text{ fm}$  (right windows): Influence of pre-equilibrium emission on isospin content of projectile (top) and target (bottom) systems. The curves show the “apparent” isospin without transfer, while the symbols denote the real isospin at separation time including also transfer. Dashed lines and open symbols correspond to asysuperstiff *EOS* and the solid lines and full symbols to the asysoft case.

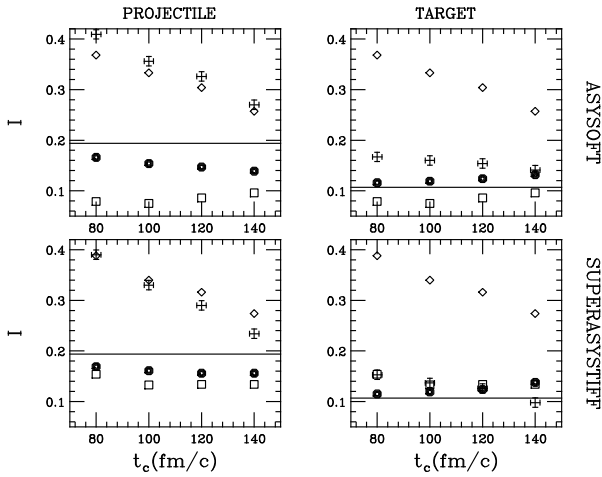


FIG. 5:  $^{124}\text{Sn} + ^{112}\text{Sn}$  collision with asysoft (top) and asysuperstiff (bottom) EOS as a function of collision time or impact parameter. Left panels:  $I_P$  (black circles),  $I_{gP}$  (crosses),  $I_{PT}$  (rhombuses) and  $I_{TP}$  (squares). Right windows:  $I_T$  (black circles),  $I_{gT}$  (crosses),  $I_{PT}$  (rhombuses) and  $I_{TP}$  (squares). The horizontal solid lines refer to the initial asymmetry of the projectile (target).

for  $b = 8\text{fm}$  ( $t_c = 120\text{fm}/c$ ) we observe that

$$I_{PT}^{(\text{asysoft})} > I_{PT}^{(\text{asysuperstiff})} > I_P^0 = 0.192 \quad (4)$$

$$I_{TP}^{(\text{asysoft})} > I_T^0 = 0.107 > I_{TP}^{(\text{asysuperstiff})} \quad (5)$$

We will show in the next chapter that the origin of these inequalities lies in the existence of the low density interface and the density dependence of symmetry energy. The asysuperstiff EOS favors the neutron migration toward the neck region from both participants. This explains why simultaneously  $I_{PT}^{(\text{asysoft})} > I_P^0$  and  $I_{TP}^{(\text{asysoft})} > I_T^0$ . We will see that for the asysoft EOS this effect is weakened.

#### IV. INTERPRETATION OF THE RESULTS

The above arguments can be made more explicit by considering that the proton and neutron migration is dictated by the spatial gradients of the corresponding chemical potentials  $\mu_{p/n}(\rho_p, \rho_n, T)$  [23]. The currents of the two species can be expressed as follows

$$\begin{aligned} j_n &= -ct\nabla\mu_n(\rho_p, \rho_n, T) = -ct\left[\left(\frac{\partial\mu_n}{\partial\rho_n}\right)_{\rho_p, T}\nabla\rho_n + \left(\frac{\partial\mu_n}{\partial\rho_p}\right)_{\rho_n, T}\nabla\rho_p\right] \\ j_p &= -ct\nabla\mu_p(\rho_p, \rho_n, T) = -ct\left[\left(\frac{\partial\mu_p}{\partial\rho_n}\right)_{\rho_p, T}\nabla\rho_n + \left(\frac{\partial\mu_p}{\partial\rho_p}\right)_{\rho_n, T}\nabla\rho_p\right] \end{aligned}$$

$$\left(\frac{\partial\mu_p}{\partial\rho_p}\right)_{\rho_n, T}\nabla\rho_p],$$

where  $ct$  is a constant. Rewriting these expressions in terms of Landau parameters,  $F_0^{qq'}$  ([3] and references therein), using:

$$N_q(T)\frac{\partial\mu_q}{\partial\rho_{q'}} = \delta_{qq'} + F_0^{qq'}, \quad q = n, p \quad q' = n, p \quad (6)$$

(where  $N_q(T)$  is the level density), we obtain:

$$\begin{aligned} j_n &= -\frac{ct}{2}([N_n^{-1}(1+I) + f_n^p + If_n^I]\nabla\rho + \rho[N_n^{-1} + f_n^I]\nabla I) \\ &= -D_n^\rho\nabla\rho - D_n^I\nabla I \end{aligned} \quad (7)$$

$$\begin{aligned} j_p &= -\frac{ct}{2}([N_p^{-1}(1-I) + f_p^p - If_p^I]\nabla\rho - \rho[N_p^{-1} + f_p^I]\nabla I) \\ &= -D_p^\rho\nabla\rho - D_p^I\nabla I, \end{aligned} \quad (8)$$

where

$$f_q^\rho = N_q^{-1}(F_0^{qq} + F_0^{qq'}) = \frac{\partial U_q}{\partial\rho_q} + \frac{\partial U_q}{\partial\rho_{q'}}, \quad (9)$$

$$f_q^I = N_q^{-1}(F_0^{qq} - F_0^{qq'}) = \frac{\partial U_q}{\partial\rho_q} - \frac{\partial U_q}{\partial\rho_{q'}}; (q \neq q') \quad (10)$$

$U_q$  is the neutron or proton mean-field potential. The second lines in eqs. (7,8) define  $p$  and  $n$  drift and diffusion coefficients due to density and isospin gradients,  $D_q^\rho$  and  $D_q^I$ , respectively. The terms  $N_q^{-1}(1 \pm I)$  and  $f_q^\rho \pm If_q^I$ , that appear in the density drift coefficients  $D_q^\rho$ , can be expressed as

$$N_q^{-1}(1 \pm I) = 2N^{-1}(\rho, T) \pm 4I\frac{\partial C_{sym}^{kin}}{\partial\rho} + O(I^2);$$

$$f_q^\rho \pm If_q^I = F(\rho) \pm 4I\frac{\partial C_{sym}^{pot}}{\partial\rho} + O(I^2), (+n, -p), \quad (11)$$

where the function  $F(\rho)$  depends only on the isoscalar part of the interaction. We have denoted by  $C_{sym}^{kin}$  and  $C_{sym}^{pot}$  the kinetic and the potential part of the symmetry energy coefficient  $C_{sym}$ , respectively. Combining eqs. (11), one can see that the isovector part of the nuclear interaction enters the coefficients  $D_q^\rho$  through the derivative of the total symmetry energy  $C_{sym}$ . On the other hand the isospin diffusion coefficients  $D_q^I$  are proportional to the quantity

$$\rho(N_q^{-1} + f_q^I) = 4[C_{sym} \pm I(\rho\frac{\partial C_{sym}}{\partial\rho} - C_{sym})], \quad (12)$$

and depend, in leading order, on the value of the symmetry energy coefficient  $C_{sym}$ .

Various particular situations can be derived from these relations. In symmetric nuclear matter  $D_n^I = -D_p^I$  and  $D_n^\rho = D_p^\rho$ . In the absence of density gradients the proton current will flow oppositely and equal in magnitude to

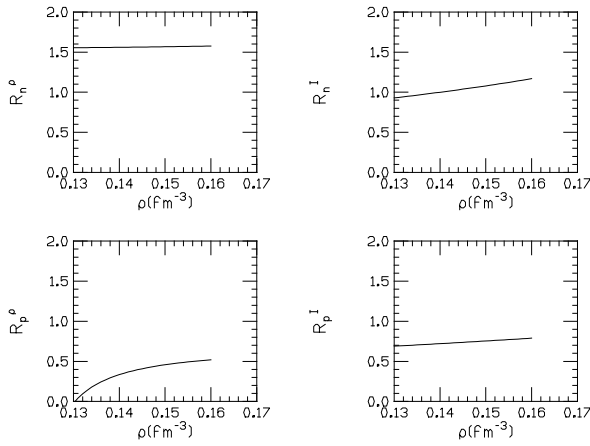


FIG. 6: Ratios of drift coefficients  $R_q^i = D_q^{i, \text{asysuperstiff}} / D_q^{i, \text{asysoft}}$ ,  $i = \rho, I$  and  $q = n, p$ , as a function of the density for fixed asymmetry  $I = 0.2$ .

the neutron current. On the other hand, for density gradients only, in asymmetric nuclear matter the proton and neutron currents may have the same direction but assume different values, inducing isospin gradients [24]. Such a situation can be encountered in semi-peripheral collisions between identical, charge asymmetric nuclei with the formation of a dilute intermediate region.

For the two asy-*EOS*'s we calculate the coefficients  $D_q^i$ ,  $i = \rho, I$  and  $q = n, p$ . We plot the ratios  $R_q^i = D_q^{i, \text{asysuperstiff}} / D_q^{i, \text{asysoft}}$  in Figure 6 as a function of the density for a fixed asymmetry  $I = 0.2$ . These values of the asymmetry and density are close to the physical conditions expected for the projectile or target region. The only negative coefficient is  $D_p^I$ . The isospin gradients, directed from the projectile to the neck and from the neck to the target, induce neutron and proton flows in opposite directions. However the ratios of the corresponding coefficients are quite close to unity for the two asy-*EOS*'s and therefore the effects are similar.

Since the density gradient is oriented from projectile and target residues to the neck, neutrons and protons migrate from higher toward lower density regions. Around and below saturation density  $R_n^\rho = D_n^{\rho, \text{asysuperstiff}} / D_n^{\rho, \text{asysoft}} > 1$  and  $R_p^\rho = D_p^{\rho, \text{asysuperstiff}} / D_p^{\rho, \text{asysoft}} < 1$ . These inequalities suggest that more neutrons and less protons migrate from projectile toward neck in the case of asysuperstiff *EOS* resulting in the formation of a more neutron rich intermediate region. This is due to the larger value of the derivative of the symmetry energy around normal density and is in agreement with the behavior observed in the numerical simulations, see eqs. (4,5).

We note that for asysuperstiff *EOS*, in spite of an enhanced isospin migration toward the neck at separation time, the projectile residue is more asymmetric in comparison to the asysoft case. One reason is that for the asy-superstiff *EOS* during the pre-equilibrium emission not

as many neutrons are removed as for the asysoft *EOS*. Also, as it was shown, for the asysuperstiff *EOS* more asymmetric matter is also transferred from the target.

We now estimate the effect of isospin transport and pre-equilibrium emission on the transport ratios. Within the following approximations

$$\frac{A_P^0}{A_P} \Big|_M \approx \frac{A_P^0}{A_P} \Big|_H \approx \frac{A_P^0}{A_P} \Big|_L ; \frac{A_{gP}}{A_P^0} \Big|_M \approx \frac{A_{gP}}{A_P^0} \Big|_H \approx \frac{A_{gP}}{A_P^0} \Big|_L \quad (13)$$

$$A_{TP} \approx A_{PT}; I_{gP}^M \approx I_{gP}^H; I_{gT}^M \approx I_{gT}^L \quad (14)$$

where the indices  $M, H, L$  refer again to the mixed (124+112), the neutron rich (124 + 124) and the neutron deficient (112 + 112) systems, we arrive at a simplified expression for the isospin transport ratio for the projectile which shows explicitly the dependence on the isospin transport ( $I_{PT} - I_{TP}$ ) and on the pre-equilibrium emission ( $I_{gP}^H - I_{gP}^L$ ):

$$R_P \approx 1 - \frac{2 \frac{A_{PT}}{A_P^0} (I_{PT} - I_{TP})}{I_P^{0,H} - I_P^{0,L} - \frac{A_{gP}}{A_P^0} (I_{gP}^H - I_{gP}^L)} \quad (15)$$

With similar approximations the target isospin transport ratio can be expressed as:

$$R_T \approx -1 + \frac{2 \frac{A_{PT}}{A_T^0} (I_{PT} - I_{TP})}{I_T^{0,H} - I_T^{0,L} - \frac{A_{gT}}{A_T^0} (I_{gT}^H - I_{gT}^L)} \quad (16)$$

It is observed that the transport ratios depend on the difference  $I_{PT} - I_{TP}$  as expected. However, in contrast to what was assumed in refs. [15, 22], it is seen that they also depend on the pre-equilibrium emission which reduces the absolute value of the transport ratios. Both effects are smaller in the case of the asysuperstiff *EOS*, for which indeed a larger  $R$  ratio is obtained.

## V. CONCLUSIONS

In this work we have studied processes related to isospin equilibration in semiperipheral collisions at Fermi energies and their dependence on the symmetry term of the *EOS*. A special feature of these reactions is the development of a low density interface between the two residues. The neck region is controlling the proton and neutron currents and their direction. The presence of density gradients also affects the isospin exchange between projectile and target and we have shown that this is sensitive to the density dependence of the symmetry energy. The neutron to proton ratio emitted during the interaction stage is also influenced by the asy-*EOS*. The interplay between the two processes leads to a stronger equilibration for asy-soft *EOS*, as it is evidenced by the isospin transport (imbalance) ratio. Actually, in the asy-stiff case, a larger isospin transfer is observed, due to

the presence of density gradients, directed from  $PLF$  and  $TLF$  towards the neck region. However, since we are studying binary processes, finally we observe a kind of compensation between the asymmetry of the matter transferred from projectile to target ( $I_{PT}$ ) and from target to projectile( $I_{TP}$ ). From this point of view, to put in better evidence effects due to the presence of density gradients, it would be more appropriate to study events where fragments originating from the neck region are also detected, possibly with their isospin content.

In the present study a rapidly increasing symmetry energy at subnormal densities (asysuperstiff) appears to be in better agreement with the existing data [15]. More recent work also considered momentum dependent inter-

actions, showing that the more repulsive character of the overall dynamics may reduce the symmetry energy stiffness required to reproduce the data [22]. The study of the interplay between the effects due to the isoscalar and isovector part of the  $EOS$  on isospin transport observables deserves further attention.

In conclusion, charge equilibration measurements in semi-peripheral heavy ion collisions at Fermi energies provide new independent observables to study the poorly known density dependence of the symmetry term of the nuclear EOS. This is of interest for other properties of asymmetric matter, like neutron skin and isovector collective response in finite nuclei, and may also be important for neutron star crust structures [3].

---

- [1] P. Danielewicz, R. Lacey, and W.C. Lynch, *Science* **298**, 1592 (2002).
- [2] *Isospin Physics in Heavy Ion Collisions at Intermediate Energies*, edited by Bao-An Li and W. Udo Schroeder, NOVA Science Publishers, Inc., New York,2001.
- [3] V. Baran, M. Colonna, V. Greco, M. DiToro, *Phys.Rep.* **410**, 235 (2005).
- [4] V. Baran et al. *Phys.Rev.Lett.* **86**, 5023 (2001).
- [5] M. Colonna, P.Chomaz, S. Ayik, *Phys.Rev.Lett.* **88**, 122701 (2002).
- [6] V. Baran et al., *Nucl. Phys.* **A703**, 603 (2002).
- [7] J.Margueron and Ph.Chomaz, *Phys. Rev.* **C67**, 041602 (2003).
- [8] H. Xu et al., *Phys.Rev.Lett.* **85**, 716 (2000).
- [9] E.Geraci et al., *Nucl. Phys.* **A732**, 173 (2004).
- [10] E.A. Uehling and G.E. Uhlenbeck, *Phys.Rev.* **43**, 552 (1933).
- [11] E.J. Hellund and E.A. Uehling, *Phys.Rev.* **56**, 818 (1939).
- [12] R.H. Anderson, C.J. Pethick, K.F. Quader, *Phys.Rev.* **B35**, 1620 (1987).
- [13] L. Shi and P. Danielewicz, *Phys.Rev.* **C68**, 064604 (2003).
- [14] M.B.Tsang, *Nucl. Phys.* **A734**, 605 (2004).
- [15] M.B.Tsang et al., *Phys.Rev.Lett.* **92**, 062701 (2004).
- [16] We note that the experimental impact parameter selection corresponds to rather peripheral collisions (estimated impact parameters  $b>8$  fm [15]). In this sense the appropriate comparison should be with  $t_c = 110-120$  fm/c interaction time simulations.
- [17] M.Colonna et al., *Nucl.Phys.* **A642**, 449 (1998).
- [18] Ph.Chomaz, M.Colonna and J.Randrup, *Phys. Rep.* **389**, 263 (2004).
- [19] V. Baran, M. Colonna, M. Di Toro, *Nucl. Phys.* **A730**, 329 (2004);  
E.De Filippo et al., *Phys. Rev.* **C71**, 044602 (2005).
- [20] M.Farine, T.Sami, B.Remaud, F.Sebille, *Z.Phys.* **A339**, 363 (1998).
- [21] F.Rami et al., *Phys.Rev.Lett.* **84**, 1120 (2000).
- [22] L.W.Chen, C.M. Ko, Bao-An Li, *Phys. Rev. Lett.* **94**, 032701 (2005); A.W. Steiner, Bao-An Li, arXiv:nucl-th/0505051.
- [23] R. Balian *From Microphysics to Macrophysics*, vol II, Springer Verlag, Berlin 1992.
- [24] We note that this is also the mechanism behind the isospin distillation (n-enrichment of the gas phase) in the liquid-gas phase transition for asymmetric matter [3, 4].